

Optical spectroscopy and initial mass function of $z = 0.4$ red galaxies

Baitian Tang^{1,2*} and Guy Worthey^{1†}

¹*Department of Physics and Astronomy, Washington State University, Pullman, WA 99163-2814, USA*

²*Departamento de Astronomía, Casilla 160-C, Universidad de Concepción, Concepción, Chile*

Accepted . Received ; in original form 2014

ABSTRACT

Spectral absorption features can be used to constrain the stellar initial mass function (IMF) in the integrated light of galaxies. Spectral indices used at low redshift are in the far red, and therefore increasingly hard to detect at higher and higher redshifts as they pass out of atmospheric transmission and CCD detector wavelength windows. We employ IMF-sensitive indices at bluer wavelengths. We stack spectra of red, quiescent galaxies around $z = 0.4$, from the DEEP2 Galaxy Redshift Survey. The $z = 0.4$ red galaxies have 2 Gyr average ages so that they cannot be passively evolving precursors of nearby galaxies. They are slightly enhanced in C and Na, and slightly depressed in Ti. Split by luminosity, the fainter half appears to be older, a result that should be checked with larger samples in the future. We uncover no evidence for IMF evolution between $z = 0.4$ and now, but we highlight the importance of sample selection, finding that an SDSS sample culled to select archetypal elliptical galaxies at $z \sim 0$ is offset toward a more bottom heavy IMF. Other samples, including our DEEP2 sample, show an offset toward a more spiral galaxy-like IMF. All samples confirm that the reddest galaxies look bottom heavy compared with bluer ones. Sample selection also influences age-color trends: red, luminous galaxies always look old and metal-rich, but the bluer ones can be more metal-poor, the same abundance, or more metal-rich, depending on how they are selected.

Key words: galaxies: abundances — galaxies: evolution — galaxies: elliptical and lenticular, cD — galaxies: luminosity function, mass function

1 INTRODUCTION

The stellar initial mass function [IMF; $\xi(m)$] is key in many active research fields, such as early universe studies, galaxy evolution, star cluster evolution, and star formation. The IMF regulates the number distribution of stellar populations as a function of mass, $dN = \xi(m) dm$, leading to impacts on the luminosity function, integrated mass to light (M/L) ratio, and number of stellar remnants. Direct IMF derivations are limited by observational capabilities and uncertainties concerning the stellar mass-luminosity relation, stellar evolution, dynamical evolution, binary fraction, counting statistics, and other factors. To make the IMF even harder to study, there is the distinct possibility that the IMF might vary in different galactic environments (Larson 1998, 2005; Marks et al. 2012; Hopkins 2013; Chabrier et al. 2014).

Salpeter (1955) described the IMF with a power-law distribution, $\xi(m) \propto m^{-\alpha}$, and adopted an IMF slope (α) of 2.35 for solar neighbourhood stars near the mass of the sun. Considering stars of very high and very low mass, the power law does not hold, and the Galactic IMF is now considered to peak at a few tenths of one solar mass (Miller & Scalo 1979; Scalo 1986; Kroupa 2001; Chabrier 2003). In terms of functional forms to model the IMF, oft-cited examples are the Kroupa (2001) series of power laws and the Chabrier (2003) log-normal distribution for $m < 1 M_{\odot}$ as representative of the log-normal probability density function of turbulent gas. Because both models are calibrated by observational data, they show a similar distribution between 0.2 and 0.8 M_{\odot} (Bastian et al. 2010; Greggio & Renzini 2012; Offner et al. 2014). A “steeper” IMF with more low mass stars is termed

* E-mail: btang@astro-udec.cl (BT)

† E-mail: gworthey@wsu.edu (GW)

¹ a power law function for $m \gtrsim 1 M_{\odot}$

bottom heavy and a “shallower” IMF with more high mass stars is termed top heavy.

Extending local studies based on counting individual stars to external galaxies, recent studies explore the universality of the IMF using integrated light and also dynamical models. Gravity-sensitive integrated spectral features such as the giant-sensitive Ca II triplet and the dwarf-sensitive Na I and FeH Wing-Ford band may indicate that systematic IMF variation exists as a function of stellar velocity dispersion (Cenarro et al. 2003; van Dokkum & Conroy 2010; Conroy & van Dokkum 2012b). This trend was fit by Ferreras et al. (2013) and Spiniello et al. (2014), but the single power law IMF slope (α) of the former study is a factor of two greater than the latter one. Minimizing the uncertainties arising from the ingredients of stellar population (SP) models appears crucial to future IMF study (Spiniello et al. 2015). Another popular approach for studying unresolved stellar systems is using dynamical models with a dark matter halo involved. The IMF is estimated by comparing the M/L ratios of the dynamical models and the stellar population models (Auger et al. 2010; Cappellari et al. 2012; Dutton et al. 2012; Posacki et al. 2015). For example, Cappellari et al. (2012) concluded an universal IMF is inconsistent with early-type galaxies (ETGs), although this kinematic result is unable to distinguish between more stellar remnants (from a top heavy IMF) and relatively more low mass stars (from a bottom heavy IMF).

Simple chemical evolution of a time-independent, bottom-heavy IMF suggests a small number of stellar remnants and also implies lower metallicities for the fossil stars. In empirical rebuttal, observations suggest super-solar metallicities in elliptical galaxies e.g., Trager et al. 2000a,b; Tang et al. 2009). Also, the number of stellar remnants is probably not small. Kim et al. (2009) suggested the number of low-mass X-ray binaries in three nearby elliptical galaxies with mass about $10^{11} M_{\odot}$ is similar to that of the Milky Way. Peacock et al. (2014) found a constant number² of black holes and neutron stars among eight different mass ETGs³. To reconcile these facts with a bottom-heavy IMF, Weidner et al. (2013a,b) simulated galaxy evolution with a time-dependent IMF, in which the IMF slope steepens as the star formation rate decreases gradually (Also see Gargiulo et al. 2015 for a semi-analytical model with similar IMF slope assumption).

IMF evolution, if it occurs in nature, may potentially be detected through studies of distant galaxies, and to possibly detect such is the motivation for the present paper. In the formation scenario that giant elliptical galaxies formed very early in cosmic history and have been passively evolving ever since, the IMF cannot change over time, though the IMF for elliptical galaxies can be very different from spiral galaxies. In the hierarchical galaxy formation picture, elliptical galaxies are the end result of merger trees that start with irregular and spiral galaxies as basic ingredients, and the elliptical galaxy should be the sum of its parts and

have an IMF similar to a spiral galaxy. Since that conclusion seems incorrect, it may be that elliptical galaxies are also subject to star formation events periodically (gas rich mergers or gas accretion) but star formation does not linger, but is rapidly quenched. In this variant of the hierarchical formation scenario, elliptical galaxies may develop their own characteristic IMF, and also, that IMF may evolve over cosmic time; early ellipticals will have a spiral-like IMF, but as time and mass-buildup goes on and they become more idiosyncratic, the elliptical galaxies may develop a distinct elliptical-flavoured IMF due to the altered star formation environment.

There is some theoretical support for expecting an evolving IMF.

1.1 IMF theories

Logically, the steeper IMFs of ETGs were either imposed at an early creation epoch or have evolved over time. Present-day ETGs are unlikely to have suffered buildups of *only* low-mass stars in the last third of the universe. We see no evidence of such an odd star formation mode ongoing, c.f. the case study of giant elliptical galaxy NGC 5128 (Neff et al. 2015), caught in a gas accretion event, which emits plenty of UV light, indicating that massive stars are forming.

Historically, the simple Jeans mass model and the turbulent Jeans mass model were influential. The simple Jeans mass model hypothesizes that the peak mass of the IMF is simply a reflection of the mean Jeans mass. For example, the Larson model (Larson 1998, 2005) showed that the Jeans mass varies either as $T^{3/2}\rho^{-1/2}$ or as $T^2P^{-1/2}$, where T is temperature, ρ is density, and P is pressure. In the early Universe, the high cosmic background temperature, low metallicity, and intense radiation from young stars and core-collapse supernova inevitably increase the proto-stellar cloud temperature. But the relation between T and ρ (or P) is still needed to estimate the Jeans mass. Larson (2005) noted the $T - \rho$ relation drawn from the observational and theoretical results of that time:

$$T = 4.4 \rho_{18}^{-0.27} K, \quad \rho < 10^{-18} \text{ g cm}^{-3} \quad (1)$$

$$T = 4.4 \rho_{18}^{+0.07} K, \quad \rho > 10^{-18} \text{ g cm}^{-3} \quad (2)$$

where ρ_{18} is the density in units of $10^{-18} \text{ g cm}^{-3}$. Therefore, Larson suggested the early universe favors a top-heavy IMF, where a low density $T - \rho$ relation was assumed.

The turbulent Jeans mass model links the characteristic mass of stars to the galactic-scale processes responsible for setting the characteristic temperatures and linewidth-size relations of molecular clouds (Krumholz 2014). The most representative models are given by Chabrier et al. (2014) and Hopkins (2013). These models are widely cited, partly due to the consistency between their model prediction and recent observations: a bottom-heavy IMF for massive early type galaxy.

However, as pointed out by Krumholz (2014), the mass of the IMF peak in the Hopkins model can be expressed as:

$$M_{peak} \approx \frac{c_s^4}{Q G^2 \Sigma} \quad (3)$$

where c_s is the sound speed, $Q \approx 1$ is the Toomre stability parameter for the disk, and Σ is the gas surface density. c_s

² Scaled by the amount of K-band stellar light covered

³ To connect black holes and other stellar remnants to the low-mass IMF posits a very coherent and simple functional form for the IMF. In nature, the high mass end of the IMF may be independent of the low mass IMF.

and Σ are both large for high surface density star formation, in which elliptical galaxies are assumed to form. The parameters may or may not imply a bottom-heavy IMF for ETGs.

1.2 IMFs observed at different redshifts

If ETGs periodically form stars, but the episodes are rapidly quenched, then most ETGs will be observed in the quiescent phases of their star formation duty cycle, and yet as a group the IMF may evolve over time. In that case, lookback studies may uncover the drift in IMF.

There is further research. Shetty & Cappellari (2014) derived the mass/light (M/L) ratios of 68 field galaxies in the redshift range of 0.7–0.9 with both dynamical modelling and stellar population modelling. The comparison of $(M/L)_{dyn}$ and $(M/L)_{pop}$ implies a Salpeter IMF, which is also possessed by nearby galaxies with similar masses. Meanwhile, Martín-Navarro et al. (2015b) studied the TiO_2 indices of a sample of 49 massive quiescent galaxies at $0.9 < z < 1.5$. The heaviest galaxies ($M_* > 10^{11.0} M_\odot$) show a bottom-heavy IMF and lighter galaxies ($10^{10.5} < M_* < 10^{11.0} M_\odot$) do not. They also concluded that the IMF of massive galaxies has remained unchanged for the last ~ 8 Gyr.

Luminosity evolution may also betray the IMF slope in that a top-heavy galaxy fades more rapidly than a galaxy with the standard IMF, since the present-day luminosity of ETG mainly comes from old stellar populations ($\sim 1 M_\odot$). According to Tinsley & Gunn (1976), the luminosity of an old stellar population is proportional to $t^{-1.6+0.3\alpha}$. Therefore, a shallower IMF implies a more dramatic luminosity change over a fixed amount of time. In that spirit, van Dokkum (2008) compared the luminosity evolution ($\Delta \log(M/L_B)$) to colour evolution ($\Delta(U-V)$) for massive galaxies in clusters at $0.02 < z < 0.83$. The luminosity evolution of these observed galaxies is faster than the trend predicted by the Maraston (2005) models with a standard IMF. Thus, the IMFs in these galaxies might be top-heavy⁴.

More support for a shallow IMF at high redshift comes from Davé (2008), who successfully brought the observed and predicted M_* –SFR relation into broad agreement by modelling the characteristic mass \hat{M} as a function of redshift: $\hat{M} = 0.5(1+z)^2 M_\odot$, where $z < 2$.

This rich variety of results is fascinating, yet ambiguous.

1.3 Observational strategy

Integrated light spectral features that are sensitive to stellar surface gravity are often used for studies of nearby galaxy IMFs. M-type giants and dwarfs emit most of their light and have important diagnostic features at red wavelengths⁵ (van Dokkum & Conroy 2010; Conroy & van Dokkum 2012b; Smith et al. 2012). However, at cosmic distances, the inevitable redshift of spectral lines and the relatively low quality of spectra obtainable beyond 1

μm increase the difficulty of measuring these features in distant objects. It motivates us to look for IMF-sensitive indices in a more accessible band. For example, the Na D, TiO_1 , and TiO_2 indices from the Lick/IDS system (Worthey et al. 1994; Trager et al. 1998) are known to be IMF-sensitive. In addition, several optical IMF-sensitive indices published by Spiniello et al. (2014) and La Barbera et al. (2013) have given us more options in index selection (Table 1).

These indices are also sensitive to population age, overall heavy element content, and altered abundance ratios in the elements that give rise to the spectral features themselves, such as Na, Ti, and Ca. Fortunately, element ratios seem fairly well constrained, judging by the good agreement on element mixture in recent papers (Johansson et al. 2012; Conroy et al. 2014; Worthey et al. 2014b). Additionally, the element sensitivity problem may be eased if multiple IMF-sensitive indices with different element sensitivities are used.

Observationally, spectra from the DEEP2 redshift survey (Newman et al. 2013), which targeted galaxies over a broad span of redshifts in the spectral range 6500 Å–9100 Å using Keck Observatory, offer themselves as an appropriate data set. The combination of spectral observations plus new spectral indicators may allow the measurement of the IMF over cosmic time.

This paper is organized as follows: The procedure of stacking DEEP2 spectra is illustrated in §2. We compare the measured indices from these composite spectra with local measurements and two different models in §4. The implications on IMF evolution are discussed in §5, and then a brief summary of the results are given in §5.1.

2 SPECTRAL REDUCTION

2.1 Sample Selection

The DEEP2 Galaxy Redshift Survey utilizes the DEIMOS multi-object spectrograph (Faber et al. 2003) on the Keck II telescope. Most of the spectra cover 6500–9100 Å, with spectral resolution $R = \lambda/\Delta\lambda \sim 6000$ (Newman et al. 2013). The optical IMF-sensitive indices are defined around 4500–6500 Å, listed in Table 1. In order to match observed and emitted spectral wavelength ranges for this index set, we chose galaxies around $z = 0.4$, corresponding to a lookback time of about 4.3 Gyr.

In detail, we selected galaxies⁶ with $0.3 \leq z \leq 0.5$ from the Data Release 4 (DR4) redshift catalog, and made sure these galaxies had photometric measurements by matching them with the DR4 photometric catalogs. The photometric data were taken with the CFH12K camera on board the 3.6-meter Canada-France-Hawaii Telescope (Coil et al. 2004). The chosen redshift range balances the number of available IMF-sensitive indices, the sample size, and the redshift similarity of our sample. Note that $z < 0.7$ galaxies were rejected during the observation in three out of the four DEEP2 fields (except the Extended Groth Strip, DEEP2 field 1), and thus galaxies at $0.3 < z < 0.5$ are less numerous than other higher-redshift samples (e.g., Schiavon et al. 2006). Next, to minimize the contribution of late type galaxies (LTGs), we

⁴ Greggio & Renzini (2012) points out that the luminosity evolution at $0 < z < 1.5$ can only constrain the IMF between $1 M_\odot$ and $1.4 M_\odot$.

⁵ e.g., $\text{Ca II } \lambda 8600$, $\text{Na I } \lambda 8190$, FeH Wing-Ford band $\lambda 9900$

⁶ Confirmed by examining the “CLASS” parameter in the catalog.

Table 1. Optical IMF-sensitive Indices

Index	Units	Blue Pseudo-continuum	Central Feature	Red Pseudo-continuum	Source
bTiO	mag	4742.750-4756.500	4758.500-4800.000	4827.875-4847.875	2
aTiO	mag	5420.000-5442.000	5445.000-5600.000	5630.000-5655.000	2
NaD	Å	5860.625-5875.625	5876.875-5909.375	5922.125-5948.125	1
TiO1	mag	5816.625-5849.125	5936.625-5994.125	6038.625-6103.625	1
TiO2	mag	6066.625-6141.625	6189.625-6272.125	6372.625-6415.125	1
TiO2 _{SDSS}	mag	6066.625-6141.625	6189.625-6272.125	6442.000-6455.000	3
CaH1	mag	6342.125-6356.500	6357.500-6401.750	6408.500-6429.750	2

1 – Worthey et al. (1994); 2 – Spiniello et al. (2014); 3 – La Barbera et al. (2013)

selected red galaxies using the galaxy colour-magnitude diagram (CMD). We plot the $(B - R)$ vs. R CMD in Figure 1. 302 galaxies have $(B - R)$ colour redder than 1.8 mag and R band magnitude brighter than $R = 22$ mag. The redshifts of these galaxies are reasonably well determined: 260 galaxies have quality code 4 (99.5% reliability rate), and 42 galaxies have quality code 3 (95% reliability rate, Newman et al. 2013).

According to Weiner et al. (2005), at $z \leq 1$, LTGs comprise about 25% of the red population. Since we lack morphology information, we cannot exclude LTGs on the basis of isophotal structure. However, we may use [O III] and $H\alpha$ emission lines to eliminate galaxies with strong emission lines (Weiner et al. 2005; Schiavon et al. 2006) and therefore ongoing star formation or active galactic nuclear activity. Based on the wavelength coverage of the deredshifted spectra, [O III] EWs⁷ can be measured in 282 galaxies. Among those, 7 galaxies have [O III] EW < -5 Å⁸. After [O III] selection, 275 galaxies are left in the sample (Sample I). Similarly, 5 out of 77 galaxies with $H\alpha$ EW measurements have $H\alpha$ EW < -5 Å, and we define thus an $H\alpha$ selected sample (Sample II) consisting of 72 galaxies.

With a large galaxy sample at $z \sim 0.9$ and a selection criteria of [O II] EW > -5 Å, Schiavon et al. (2006) estimated the LTG proportion of their sample is at most 5%. Though there is similarity between our selection method and theirs, our sample size is smaller and less complete, thus we estimate the LTG portion of our sample is 5–25%, between the predictions of Schiavon et al. (2006) and Weiner et al. (2005).

Besides a few bright, red LTGs in the sample, there may also be some low power AGN. The Baldwin–Phillips–Terlevich (BPT) diagnostic diagram (Baldwin et al. 1981) suggested that [O III] EW < -5 Å, or $H\alpha$ EW < -5 Å, which is used as one of our sample selection criteria, cannot effectively eliminate the AGN contributions.

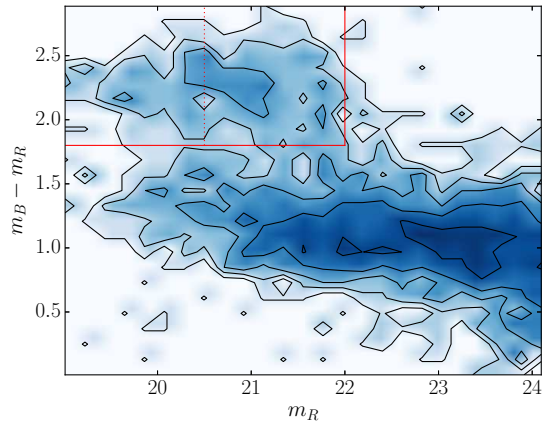


Figure 1. Galaxy colour magnitude diagram. Darker blue regions have greater number density. The red sequence is the peak in the upper left, the blue cloud is the peak at lower right, and the green valley is the low density gap between. The red galaxies are selected by $m_R < 22$ mag (vertical red line), and $m_B - m_R > 1.8$ mag (horizontal red line). A magnitude cut for subsampling was made at $m_R = 20.5$ mag (vertical dotted red line).

2.2 Composite Spectra and Index Measurements

We retrieved the one dimensional spectra from the DEEP2 Data Release 4 website⁹. The reduced two dimensional spectra obtained from DEIMOS are flat-corrected and wavelength-calibrated. The pipeline also takes care of the sky subtraction and cosmic ray rejection. One dimensional spectra are extracted from each of the slitlets using an optimal extraction method (Horne 1986) that assumes a constant Gaussian profile at all wavelengths, which implies the spectral extraction region is the whole visible galaxy. Flux calibration is not attempted along the process, and the flux unit is DEIMOS counts per hour (e^- /hour).

To stack the spectra we used pipeline programs developed by the DEEP2 team (Cooper et al. 2012). We modified the “coadd_spectra” program to meet our (mild) need for flux correction. In measuring spectral indices, scalings and even linear corrections do not affect the result. However, if the response curve correction is more complicated than linear, there is a mild effect, and so we included the flux correction. We divided each spectrum by the throughput of

⁷ Defined in González (1993)

⁸ Weiner et al. (2005) showed the median error in rest-frame EW is 6.2 Å. Schiavon et al. (2006) suggested -5 Å for the EW limit, though they use [O II] due to a different rest-frame wavelength range.

⁹ <http://deep.ps.uci.edu/DR4/spectra.html>

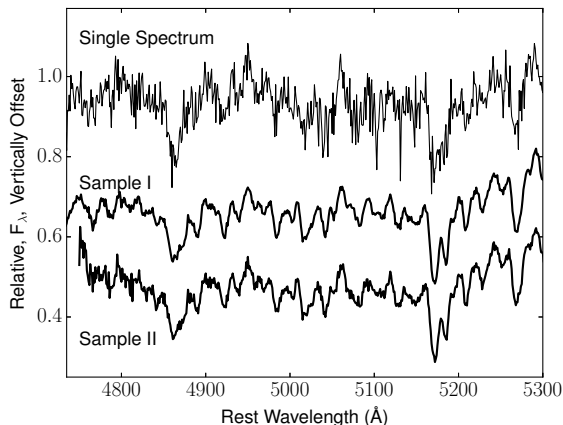


Figure 2. A swath of DEEP2 spectra before and after stacking to illustrate S/N improvement. Sample I stacks 275 spectra, and Sample II stacks 72 spectra to achieve higher S/N at cost of the loss of individual galaxy identities.

DEIMOS in spectroscopic mode for the gold 1200-line/mm grating¹⁰. Next, each individual spectrum is shifted to the rest-frame and normalized by dividing the median spectrum. The composite spectra are achieved by coadding the normalized spectra, where the inverse variance of each pixel is used as weight (see Figure 2).

We estimated the velocity dispersions (σ) of the composite spectra in two ways; the Faber & Jackson (1976) $\sigma-L$ scaling relation and cross-correlation. For luminosity, we K-corrected the R band magnitude to B band magnitude using the code of Blanton & Roweis (2007). The velocity dispersion was calculated by adopting the Faber-Jackson relation presented in Whitmore & Kirshner (1981). The average σ of our 302 red galaxy pool is about 235 ± 40 km s⁻¹. For the latter estimate, we cross-correlated the composite spectra with model stellar spectrum templates, with the width of the cross-correlation function fitted with a Gaussian and treated as in Tonry & Davis (1979). Composite spectra of Sample I and Sample II show $\sigma \sim 241$ km s⁻¹, and ~ 231 km s⁻¹, respectively. The velocity dispersions determined by these two methods agree.

We broadened the spectra to 300 km s⁻¹ ($\sigma_{broaden}^2 = \sigma_{300}^2 - \sigma_{sample}^2$), and measured spectral indices and associated errors propagated from the errors on each flux pint. In terms of studying indices rather than the spectra directly, we chose indices because more theoretical predictions are available, systematic fluxing issues are minimized, and analysis is more secure and direct. Our index table consists of Lick-style indices presented in Worthey et al. (1994); Trager et al. (1998); Serven et al. (2005), and Table 1. The measured indices and errors are shown as red (Sample I) and light grey (Sample II) filled circles with error bars in Figure 4. The errors plotted are pixel by pixel measurement errors propagated through to the indices (and do not include a contribution from velocity dispersion uncertainty that modestly affects narrower indices).

The H β index was corrected for emission via the meth-

ods in Serven & Worthey (2010), that is, via measurement of an H α index, then using Mg *b* to estimate a continuum slope correction. The corrections were substantial since the stacked H α indices were generally in emission, from 0.5 Å for the low-luminosity subsample up to 1.1 Å for high luminosity.

We also subdivide the sample by luminosity at $m_R = 20.5$ mag. Cross-correlation indicates a 15% smaller velocity dispersion in the faint subsample and a 5% larger velocity dispersion in the bright subsample compared to the average. These differences were propagated through the smoothing and index measurement procedures.

3 MODELS AND LOCAL OBSERVABLES FOR COMPARISON

Stellar population model information and additional observational material is needed for a fair comparison of IMF indicators.

Worthey models: Models (Worthey 1994; Trager et al. 1998) that start with empirical stellar libraries, then use synthetic spectra (Lee et al. 2009) to gauge the effects of detailed chemical composition were employed, with a few ongoing improvements.

For this version, the isochrones of Bertelli et al. (2008, 2009) with the thermally-pulsing asymptotic giant branch (TP-AGB) treatment described in Marigo et al. (2008) were employed. This set of isochrones has a low mass limit of 0.15 M $_{\odot}$. In philosophy similar to Poole et al. (2010), indices were measured from four stellar spectral libraries (Valdes et al. 2004; Worthey et al. 2014a; Sánchez-Blázquez et al. 2006; Rayner et al. 2009), all transformed to a common 200 km s⁻¹ spectral resolution. Multivariate polynomials were fit over five overlapping temperature zones as a function of $\theta_{eff} = 5040/T_{eff}$, log *g*, and [Fe/H], then smoothed and summarized in a lookup table. To compute the integrated properties of the final model, the isochrones plus an IMF give the numbers of stars in each bin of the isochrone. The stellar index was found (and any optional chemical element tweaks imposed), then decomposed into “index” and “continuum” fluxes, which were separately added, then, after summation, re-formed into an index representing the integrated value. To transform from 200 km s⁻¹ to 300 km s⁻¹ small additive corrections for each index were estimated by Gaussian-broadening high resolution synthetic composite spectra.

For this work, we updated the models with additional IMF options. We calculate SSP models with the Kroupa (2001) IMF to represent LTGs and two power law IMF slopes: $\alpha = 2.35, 3.0$. For each IMF slope, our SSP models are given at the ages of 5, 10 Gyr, with [M/H] = {−0.33, 0, 0.37}.

CvD12: We also employ the Stellar Population Synthesis (SPS) presented in Conroy & van Dokkum (2012a) (CvD12). CvD12 models scaled-solar old stellar populations (>3 Gyr) with empirical spectral libraries: MILES (Sánchez-Blázquez et al. 2006) and IRTF (Cushing et al. 2005; Rayner et al. 2009). Within the limitation of near-solar abundance, they also probe individual abundance variations and α element enhancements with synthetic spectral libraries as well as provide IMF variation options. For

¹⁰ <http://www.ucolick.org/~ripisc/results.html>

our illustrations, we adopt the spectra presented in CvD12 from <http://scholar.harvard.edu/cconroy/sps-models>. These spectra are the SPS model output at four ages (3, 5, 7, and 9 Gyr) with four different types of IMFs ($\alpha = 3.5$, $\alpha = 3.0$, Salpeter, and Chabrier). We measured indices after we broadened the spectra to 300 km s^{-1} .

Local galaxies: As stellar population models still suffer from uncertainties (Charlot et al. 1996; Conroy et al. 2009; Tang et al. 2014), local galaxies are useful for empirical comparison. Since our sample galaxies consists of a majority of ETGs and a few LTGs, templates of both galaxy types are desired. Note that spectra from all sources were broadened to 300 km s^{-1} for purposes of comparison.

(i) We were kindly provided with the updated mean spectra of non-star forming, non-LINER galaxies by G. Graves. Galaxies from SDSS DR7 were selected with the following criterion: (1) $0.025 < z < 0.06$; (2) No detectable $\text{H}\alpha$ or $[\text{O II}] 3727$ emission (Peek & Graves 2010); (3) Median $S/N > 5$ per \AA . Then, the galaxies were divided into six bins in $\log \sigma$: 1.86–2.00, 2.00–2.09, 2.09–2.18, 2.18–2.27, 2.27–2.36, 2.36–2.50; (4) further culling if the galaxies were far from the fundamental plane. See Conroy et al. (2014) for a more detailed description of the sample, where the last velocity dispersion bin of our sample are sub-divided into two. Finally, $\text{H}\beta$ was corrected via Serven & Worthey (2010).

(ii) Dobos et al. (2012) classified the galaxies of SDSS DR7 by both colour and nuclear activity. We select the two most relevant subsamples: 1) The passive galaxies (with no $\text{H}\alpha$ detection) split by color into red, green, and blue sub-samples, and 2) a red sample, sub-divided into five smaller samples based on nuclear activity from low to high: (Their RED 1, RED 2, RED 3, RED 4, and RED 5 samples). In order to avoid Malmquist bias, each sub-sample is constrained by redshift and absolute magnitude to ensure volume-limited sampling. The detailed redshift and absolute magnitude ranges can be found in their Table 2. For example, the passive samples are selected inside $0.03 < z < 0.14$, $-20.5 < M_r < -21.5$. Note that this sample is more distant than the Graves sample. Applying the Faber-Jackson law to this sample, we infer velocity dispersions around 142 km s^{-1} with narrow variance, so we adopt this value for purposes of correcting to 300 km s^{-1} for all the subsamples. $\text{H}\beta$ corrections were applied similar to the DEEP2 sample. Note that the Dobos passive sample's selection criteria are the most similar to our DEEP2 galaxies. This point becomes important when we discuss IMF evolution.

(iii) We also retrieved the Sb galaxy template from Kinney et al. (1996). This optical template is a combination of two Sb galaxies, NGC 210 and NGC 7083, whose spectra were obtained at the CTIO 1 m telescope with the two-dimensional Frutti detector. The CTIO spectra covers $3200\text{--}10000 \text{ \AA}$ with a resolution of 8 \AA , which was then smoothed to 300 km s^{-1} with a smoothing kernel that varies with wavelength. $\text{H}\beta$ corrections were applied similar to the DEEP2 sample.

4 RESULTS

Figures 3 and 4 intercompare index values from the models and the observations. The $[\text{MgFe}]^{11}$ is chosen as the x -axis variable since it tracks mostly $[\text{M}/\text{H}]$ rather than $[\alpha/\text{H}]$ or $[\text{Fe}/\text{H}]$, though it retains considerable sensitivity to population age.

Examining Fig. 3, the top-left panel shows age-sensitive $\text{H}\beta$. The model grid show two isochrons at 2, 5, and 10 Gyr with dots at $[\text{M}/\text{H}] = -0.33, 0.0, \text{ and } 0.37$. Grid extrapolations are approximately linear. Variable IMF models are not shown in Fig. 3, and the IMF is a power law with low mass cutoff of $0.15 M_{\odot}$. The DEEP2 galaxies are marked with circles and error bars. The two sample grand averages, marked with larger circles, are flanked by smaller circles that represent a split of the sample at $R = 20.5$. This is approximately half by number, although the fainter half has larger errors. The Graves passive galaxies (open black diamonds representing a series of bins in velocity dispersion), Dobos passive galaxies (open triangles representing three color bins), and Dobos RED galaxies (open stars representing AGN activity increasing from small symbols to large symbols) are also plotted.

In terms of velocity dispersions, the Dobos galaxies locate about the 3rd (from the left) Graves bin, while the DEEP2 galaxies locate between the 5th and 6th. The DEEP2 galaxies should be younger by ~ 4.3 Gyr due to lookback time, all else being equal. The $\text{H}\beta$ emission corrections for the active galaxies are more uncertain because the corrections (Serven & Worthey 2010) were built for star formation scenarios, not AGN.

The trends apparent in the $\text{H}\beta$ diagram are that more massive/redder galaxies appear older and more metal rich relative to the model grid, a trend seen since the invention of this diagnostic diagram (Faber et al. 1992). There appears to be only one contradiction apparent in the $\text{H}\beta$ diagram, which is that the Dobos sequences might be expected to cross the Graves sequence at the third diamond (matching velocity dispersions), not converge at the 6th, as observed. However, that is only a contradiction if the samples are expected to be equivalent. If we posit that sample selection can have an influence, then what we see are diagnostics of the sample selection method. Points to note in the $\text{H}\beta$ diagram:

- ETGs form a narrow sequence in $[\text{M}/\text{H}]$ but range over a large range of average age.
- The LTG template had a large nebular emission correction, but within that uncertainty appears to be of intermediate age but a few tenths more metal poor than the ETGs.
- The three samples (Graves nonLINER, Dobos Passive, Dobos Red) tilt progressively such that the bluer Graves galaxies are more metal poor, the bluer Dobos Passive galaxies are on an isometallicity track, and the bluer Dobos Red galaxies (the least AGN active) are more metal rich.
- The DEEP2 samples lie slightly more metal rich from the convergent red end of the other samples, but much younger. The youthening effect is much stronger than passive evolution.

¹¹ $[\text{MgFe}] \equiv \sqrt{\text{Mg } b * (\text{Fe}5270 + \text{Fe}5335)/2}$, from González (1993)

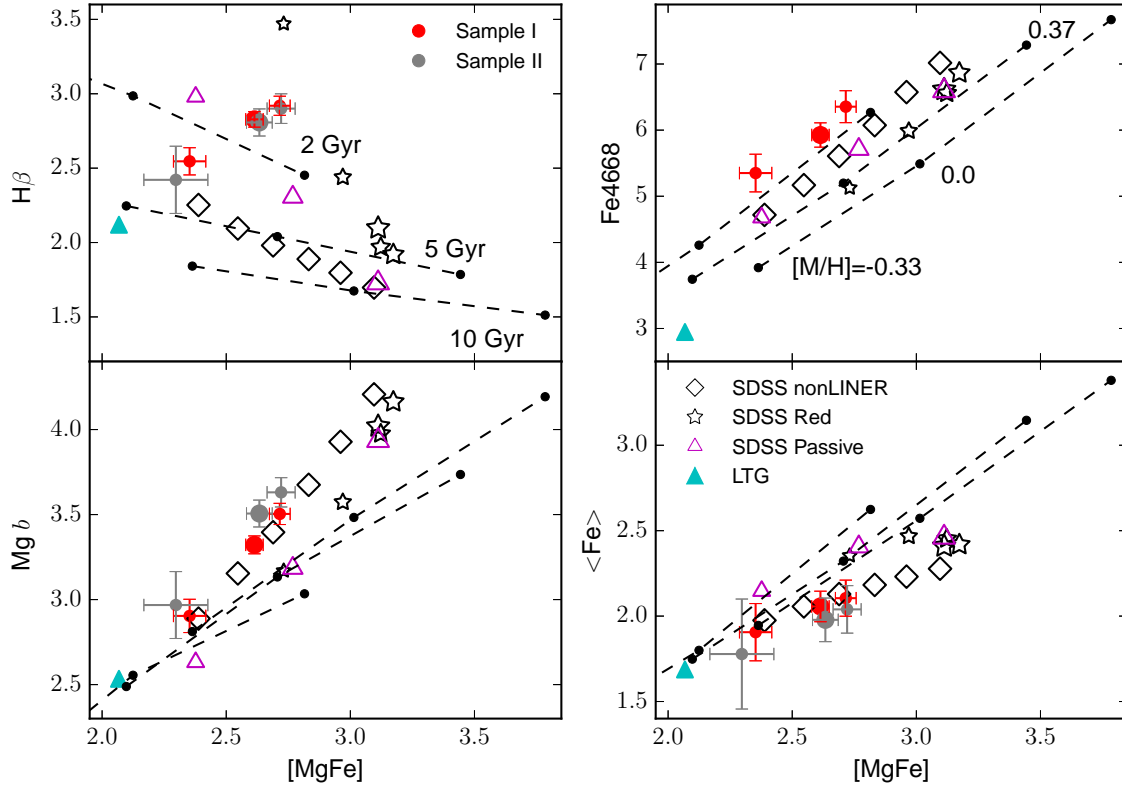


Figure 3. Index planes that are not sensitive to the IMF. They show expected age and abundance trends for the most part. Our SSP models are given at age= 2, 5, and 10 Gyr with $[M/H] = -0.33, 0, \text{ and } 0.37$ (dashed tracks). The observables are the Graves non-LINER averages binned by velocity dispersion (open diamonds), Dobos Passive split into three color bins (open magenta triangles), Dobos RED split by nuclear activity (black five-pointed stars; the smallest nuclear activity, the largest the most), Kinney LTG (cyan filled triangle), $[O\text{III}]$ selected Sample I (red filled circles), and $H\alpha$ selected Sample II (grey filled circles). Each Sample I/II grand average is indicated by a larger symbol, and the smaller symbols indicate a split in the sample at magnitude $m_r = 20.5$.

Moving to the other three panels of Fig. 3, these are diagrams typically used to track abundance ratio changes because they are age-metallicity degenerate (Worthey 1998). The usual conclusion is that smaller ETGs resemble LTGs in their abundance ratios, and that these ratios are scaled-solar. From there, the massive ETGs show enhanced Mg and other light elements, while Fe-peak elements are depressed relative to the average. These trends are confirmed here. It is statistically significant that, except for the reddest few, the Dobos samples are a bit more Fe-rich, Mg-poor, also lie low in Fe4668, which is mostly due to carbon. This must be sample selection. Mentally allowing for the age difference, which weakens all the metallic feature indices, the DEEP2 sample shares the typical abundance pattern of massive ETGs.

Fig. 4 shows IMF-sensitive indices. In both sets of models, a young population age decreases sensitivity to IMF. The two sets of models agree qualitatively, though the present model set is always shifted a bit more strong-lined than CvD12. In all the various indices pictured, shallow IMFs imply weaker feature strengths¹². Looking at the diagrams

empirically, except for the least-diagnostic Na D panel, the Graves sequence is stronger-lined in all IMF diagnostics. The empirical points seem to split into two families, with the Graves sample defining one, and all the others, including the LTG template, Dobos samples and DEEP2 ETGs, defining the other. That the Dobos samples and DEEP2 ETGs share the same shallow IMF indicates little cosmic evolution in IMF over the last 4 Gyr.

For disentangling possible age effects, perhaps the best diagrams are the TiO2 and TiO2-SDSS indices, because the models begin to develop strong AGBs at younger ages so that the models never dip weak enough to reach the observed DEEP2 or Dobos indices unless the IMF is shallow. For disentangling abundance ratio effects, we look for the various TiO diagrams to be echoed in the Mg4780 diagram. The morphology is the same, and we conclude that IMF may play a role in the index strengths.

The Na D index has a small amount of IMF sensitivity,

SDSS indices. This is because the IMF effects in young, metal-poor populations and old, metal-rich populations are dominated by stars from different stellar phases. Readers are referred to Tang & Worthey (2015) for more details.

¹² Exceptions to this general behaviour is found in the youngest and most metal-poor populations for TiO1, TiO2, and TiO2-

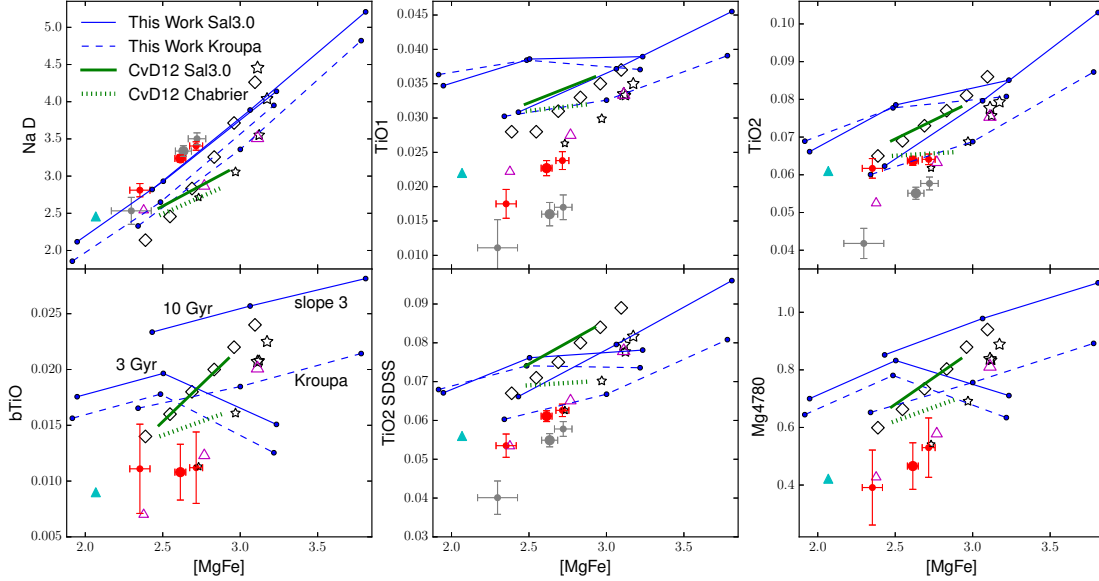


Figure 4. Index planes that are sensitive to the IMF. Most symbols are as in Fig. 3. The selection of models is altered, however. Our SSP models are shown for ages 3 and 10 Gyr, and for a bottom-heavy $\alpha = 3.0$ power-law IMF (solid blue lines) and a Kroupa IMF (dashed blue lines) that is similar to the Chabrier IMF. In addition, CvD12 models are given with lines connecting ages 3 and 9 Gyr at solar metallicity. An $\alpha = 3.0$ power-law IMF (solid green line) and a Chabrier IMF (dotted green line) give the IMF sensitivity. If both sets of models agreed perfectly, the CvD12 models would nearly connect the middle two dots on the metallicity-sensitive model isochrones.

but it has a large amount of sensitivity to abundance ratios. It may also, especially in the cases of the LTG template and the DEEP2 sample, suffer from galaxy self-absorption if neutral Na is present in the interstellar medium, since both the component of Na D are resonance lines. The Graves and Dobos sequences tilt such that more massive ETGs have a steeper IMF than the lightweight ones.

5 DISCUSSION, SUMMARY, AND CONCLUSION

Random uncertainties are shown in Figs. 3 and 4 except that the random uncertainties are smaller than the point symbols for all the SDSS averages and could not be estimated with certainty for the LTG template, but are plausibly of order 0.1 Å or 0.005 mag.

Systematic uncertainties are a bigger worry. Velocity dispersion corrections are important for $H\beta$, Mg b , $\langle Fe \rangle$, Na D, and Mg4780, but a much lesser concern for Fe4668 and the four TiO indices. Corrections were applied to all indices, however, so the primary uncertainty is the difficulty of knowing the appropriate velocity dispersion to assign to each averaged bin, weighted by how close the galaxy bin is to the target 300 km s⁻¹, because the closer the galaxy is to that target, the smaller the correction. We judge that the only data points that might suffer a significantly skewed result are the low-luminosity subsamples from DEEP2. There are additional systematics for the $H\beta$ diagram due to emission corrections, as discussed above, and a small worry for extra Na D self-absorption, a few tenths of an Angstrom at

most (Blades & Morton 1983; Bica & Alloin 1986). Milky Way Na absorption is not an issue due to the redshifts of the galaxies. The most serious uncontrolled systematic effect is likely to be spectrophotometric integrity. If spectral response curvatures the same order as the index widths occur, and are not averaged away, they will produce spurious unastrophysical drifts in the indices. The fluxing procedures in DEEP2 and the averaging in SDSS samples will minimize this. The indices most prone to fluxing errors are TiO1, TiO2, and TiO2-SDSS due to their long wavelength spans. Indeed, it is in these indices that Sample I and Sample II diverge strongly, and that is probably no coincidence.

Systematic effects in the models are likely to be more severe. Fluxing should not be a problem, but velocity dispersion corrections must be made. Furthermore, besides simplified, parameterized IMFs, the models are based on stellar evolutionary models which, while admirable in many ways, are also prone to uncontrolled drifts in stellar temperatures, luminosities, and lifetimes (Charlot et al. 1996). We recommend eyeing the models only in a differential sense, looking for the vectors of age, $[M/H]$, and IMF in the various index-index diagrams.

A few additional considerations deserve a few words. Tang & Worthey (2015) studied two effects that might entangle with the IMF slope determination, namely the IMF Low Mass Cut-Off (LMCO), and AGB contribution effects. The degeneracies between slope, LMCO, and AGB star contributions are real, but testing indicates they are too subtle to affect the appearance of Fig. 4.

In ETGs, $[Ti/Fe] \approx 0$ (Johansson et al. 2012; Conroy et al. 2014; Worthey et al. 2014b). Could Ti be even

more underabundant in our galaxies? Additional indices Ti4553 and Ti5000 (not illustrated and not sensitive to the IMF) lie slightly lower than solar for our sample galaxies. Thus the small values of Ti-related indices may be partially due to the low Ti abundances. However, sub-solar Ti abundances can only explain indices containing Ti. The Mg4780 index is not Ti-sensitive, yet indicates a shallower IMF even without accounting for Mg-enhancement. Mg4780 is defined in Serven et al. (2005), and shown to be IMF-sensitive in La Barbera et al. (2013). Our models accommodate varying Mg and Ti separately, but testing with abundance-altered models fails to indicate any easy way to relieve the appearance that shallow IMFs are required in Fig. 4.

Since the SDSS spectra are limited to the galaxy center by the fixed fiber size (3 arcsec), the relatively nearby ($0.025 < z < 0.06$) Graves stack may be biased towards the stellar populations in the galaxy center. The Dobos samples are less affected by the aperture effect, since the sampling galaxies are on average further away ($0.03 < z < 0.14$ for the passive samples). For the DEEP2 samples, the long-slit spectroscopy and the optimal extraction method ensure that the DEEP2 spectra are free from aperture effect. According to the recent work of the MaNGA team on stellar population gradients (Zheng et al. 2016; Goddard et al. 2016), no or slightly negative metallicity gradients are found in a large sample of nearby galaxies, though the metallicity gradients may be stronger in more narrowly selected massive ETGs (van Dokkum et al. 2016). Therefore, the Graves stack measurements with larger σ may be slightly affected by the metallicity gradient. The correcting vectors should point to the lower-left corner of the panels in Figure 4, indicated by our SSP models (blue lines). Furthermore, the IMF gradients suggested by Martín-Navarro et al. (2015a); van Dokkum et al. (2016) may also affect the Graves stack measurements with larger σ , thus the aperture effect may magnify the IMF-related indices.

5.1 Summary

With these caveats in mind, the firm conclusions of examining Figs. 3 and 4 are

- Sample selection strongly drives every diagnostic diagram.
- The brightest, reddest galaxies are the oldest on average. From there, however, sample selection drives a newly seen trend for age. In the sample selected by ETG fundamental plane, bluer galaxies are more metal-poor. In a sample composed purely of non-AGN, non-star-forming galaxies, bluer galaxies are the same metallicity as red ones but much younger. In a sample with detectable AGN activity, the bluer galaxies are more metal rich, and that partially anticorrelates with AGN activity; the least-active galaxies are both younger and more metal rich.
- To explain all the index drifts in comparison to the models, IMF variations seems to be required, along with age and abundance variations. In all SDSS averages there is trend that the strongest lined galaxies appear to have a more bottom heavy IMF, while the weaker lined galaxies have a spiral-like bottom light IMF, in accord with many recent studies.

- The SDSS sample that is culled to be near the fundamental plane of ETGs and thus is probably the purest in terms of ETG fraction forms a separate sequence that is offset toward a bottom-heavy IMF. The other SDSS samples that likely contain more LTGs group with the similarly-selected DEEP2 samples and the LTG template galaxy itself for a sequence at a more bottom-light location.

- Split by luminosity, the low-luminosity half of the DEEP2 red galaxy sample is slightly more metal-poor, which is expected if metallicity drives the color-magnitude relation, but also older on average, which is an interesting new result that should be confirmed when more and better spectra of high redshift galaxies are available.

- The DEEP2 samples appear to be slightly enhanced in carbon (Fe4668 index) and sodium (Na D index) and quite possibly slightly deficient in titanium (the various TiO indices) compared to their zero-redshift cohorts.

- The DEEP2 samples are about a factor of two younger than would be inferred if they were the passively evolving precursors of the nearby strong-lined galaxies. That is, in Fig. 3, galaxies at the DEEP2 velocity dispersion have ages around 8 Gyr, the DEEP2 galaxies have ages less than 2 Gyr, and the lookback time is roughly 4 Gyr.

- Since the DEEP2 samples mesh with similarly-selected nearby galaxies (the Dobos samples), we do not find evidence of cosmic evolution in IMF over the last 4 Gyr. However, our fidelity at detecting IMF variations is low, and such evolution could exist at a modest level.

5.2 Future Improvements

The spectroscopic study of IMF cosmic evolution can be improved in several ways:

(i) Studying galaxies at higher redshift would presumably accentuate trends seen at less extreme lookback times. Given that DEEP2 Galaxy Redshift Survey is designed for galaxies at $z \sim 1$, the wavelength range we see is the near-ultraviolet. Finding IMF-sensitive indices in the ultraviolet, however, is formidable, if not impossible, since the diagnostic cool stars emit only a small percentage of their light there.

(ii) Alternatively, keeping to modest redshifts of $0.3 < z < 0.5$, a larger sample would increase the S/N ratio of the composite spectra and allow subdivision of samples to better characterize any IMF evolution. Morphological classification, fundamental plane subselections, and AGN information would improve the certainty of what sort of objects are under study. SDSS-BOSS (Ross et al. 2016) could be mined, for example.

(iii) Spectroscopic study of the IMF in the J band has recently become possible, and has been successful (Smith et al. 2015). At $z=0.4$, the Na I and Ca II features would fall into the J-band, therefore these classical feature lines can be used for future cosmic evolution study.

(iv) Targeting individual distant galaxies at high S/N would yield information on galaxy to galaxy cosmic scatter in IMF parameters, as well as age and abundances, perhaps revealing a whole new level of detail about galaxy evolution. It may be feasible to observe a sample of bright galaxies in a cluster with a multiplexed instrument (e.g., VLT/KMOS or Keck/MOSFIRE) in a reasonable time.

5.3 Conclusion

Recent research on nearby galaxies suggests variable IMFs and questions the universality of the IMF seen around the solar neighbourhood. In particular, massive elliptical galaxies appear to have a bottom-heavy IMF in comparison to low-mass elliptical or spiral galaxies. For high-redshift galaxies, the red IMF-sensitive indices shift out of the CCD wavelength range. In this paper, we apply a set of bluer IMF-sensitive indices to the studies of intermediate-redshift ($0.3 < z < 0.5$) galaxies. Red galaxies are selected from the DEEP2 Galaxy Redshift Survey and stacked. Spectral indices measured from the composite spectra are compared with two sets of models and also local galaxies.

We confirm recent work that strong-lined (red, massive) galaxies appear to have a bottom-heavy IMF compared to weak-lined ETGs and LTGs. There is an affirming additional trend that the local sample that culls out fundamental plane outliers and thus selects what we think of as elliptical galaxies the best is offset from samples that are selected in more inclusive ways, in the sense that the pure-E sample is offset toward a more bottom-heavy IMF. The DEEP2 galaxies do not appear that bottom-heavy, joining local LTGs and similarly-selected SDSS averages. There is no evidence for evolution in the IMF over the last 4 Gyr, at least with current data and tools.

In terms of ages and abundances for local galaxies, sample selection drives a fascinating trend in which all of the reddest galaxies converge at metal-rich and old, but bluer galaxies do not agree: fundamental plane culled blue galaxies lie more metal poor and a bit younger, zero-nebula selected blue galaxies lie at the same abundance but much younger, and the bluest bins of red galaxies with detectable AGN lie much younger and *more* metal rich.

The DEEP2 red galaxies, if split in half by luminosity, show that the faint half is more metal poor, and, surprisingly, older. This trend may be driven by small number statistics. The DEEP2 red galaxies are also quite young, less than 2 Gyr, as compared to 8 Gyr for local galaxies at the same velocity dispersion, effectively ruling out a passive evolution hypothesis. The DEEP2 red galaxies are likely slightly enhanced in C and Na and slightly deficient in Ti.

6 ACKNOWLEDGEMENT

B. T. would like to thank Y. Chen for her help on the DEEP2 spectral reduction and J. Newman and R. Yan for useful technical advice. We thank the referee, Russell Smith, for insightful comments. Support to G. W. for program AR-13900 was provided by NASA through a grant from the Space Telescope Science Institute, which is operated by the Association of Universities for Research in Astronomy, Inc., under NASA contract NAS 5-26555.

REFERENCES

Auger M. W., Treu T., Gavazzi R., Bolton A. S., Koopmans L. V. E., Marshall P. J., 2010, *Astrophys J. Letters*, 721, L163
 Baldwin J. A., Phillips M. M., Terlevich R., 1981, *Pub. Astron. Soc. Pacific*, 93, 5

Bastian N., Covey K. R., Meyer M. R., 2010, *Annual Review of Astronomy and Astrophysics*, 48, 339
 Bertelli G., Girardi L., Marigo P., Nasi E., 2008, *Astron. Astrophys.*, 484, 815
 Bertelli G., Nasi E., Girardi L., Marigo P., 2009, *Astron. Astrophys.*, 508, 355
 Bica E., Alloin D., 1986, *Astron. Astrophys.*, 166, 83
 Blades J. C., Morton D. C., 1983, *Monthly Notices Royal Astron. Soc.*, 204, 317
 Blanton M. R., Roweis S., 2007, *Astron. J.*, 133, 734
 Cappellari M., McDermid R. M., Alatalo K., Blitz L., Bois M., Bournaud F., Bureau M., Crocker A. F., Davies R. L., Davis T. A., de Zeeuw P. T., Duc P.-A., Emsellem E., Khochfar S., Krajnović D., Kuntschner H., Lablanche P.-Y., Morganti R., Naab T., Oosterloo T., Sarzi M., Scott N., Serra P., Weijmans A.-M., Young L. M., 2012, *Nature*, 484, 485
 Cenarro A. J., Gorgas J., Vazdekis A., Cardiel N., Peletier R. F., 2003, *Monthly Notices Royal Astron. Soc.*, 339, L12
 Chabrier G., 2003, *Pub. Astron. Soc. Pacific*, 115, 763
 Chabrier G., Hennebelle P., Charlot S., 2014, *Astrophys J.*, 796, 75
 Charlot S., Worthey G., Bressan A., 1996, *Astrophys J.*, 457, 625
 Coil A. L., Newman J. A., Kaiser N., Davis M., Ma C.-P., Kocevski D. D., Koo D. C., 2004, *Astrophys J.*, 617, 765
 Conroy C., Graves G. J., van Dokkum P. G., 2014, *Astrophys J.*, 780, 33
 Conroy C., Gunn J. E., White M., 2009, *Astrophys J.*, 699, 486
 Conroy C., van Dokkum P., 2012a, *Astrophys J.*, 747, 69
 Conroy C., van Dokkum P. G., 2012b, *Astrophys J.*, 760, 71
 Cooper M. C., Newman J. A., Davis M., Finkbeiner D. P., Gerke B. F., 2012, *spec2d: DEEP2 DEIMOS Spectral Pipeline*. Astrophysics Source Code Library
 Cushing M. C., Rayner J. T., Vacca W. D., 2005, *Astrophys J.*, 623, 1115
 Davé R., 2008, *Monthly Notices Royal Astron. Soc.*, 385, 147
 Dobos L., Csabai I., Yip C.-W., Budavári T., Wild V., Szalay A. S., 2012, *Monthly Notices Royal Astron. Soc.*, 420, 1217
 Dutton A. A., Mendel J. T., Simard L., 2012, *Monthly Notices Royal Astron. Soc.*, 422, L33
 Faber S. M., Jackson R. E., 1976, *Astrophys J.*, 204, 668
 Faber S. M., Phillips A. C., Kibrick R. I., Alcott B., Allen S. L., Burrous J., Cantrall T., Clarke D., Coil A. L., Cowley D. J., Davis M., Deich W. T. S., Dietsch K., Gilmore D. K., Harper C. A., Hilyard D. F., Lewis J. P., McVeigh M., Newman J., Osborne J., Schiavon R., Stover R. J., Tucker D., Wallace V., Wei M., Wirth G., Wright C. A., 2003, in *Society of Photo-Optical Instrumentation Engineers (SPIE) Conference Series*, Vol. 4841, *Instrument Design and Performance for Optical/Infrared Ground-based Telescopes*, Iye M., Moorwood A. F. M., eds., pp. 1657–1669
 Faber S. M., Worthey G., Gonzales J. J., 1992, in *IAU Symposium*, Vol. 149, *The Stellar Populations of Galaxies*, Barbuy B., Renzini A., eds., p. 255
 Ferreras I., La Barbera F., de la Rosa I. G., Vazdekis A., de Carvalho R. R., Falcón-Barroso J., Ricciardelli E., 2013,

- Monthly Notices Royal Astron. Soc.*, 429, L15
- Gargiulo I. D., Cora S. A., Padilla N. D., Muñoz Arancibia A. M., Ruiz A. N., Orsi A. A., Tecce T. E., Weidner C., Bruzual G., 2015, *Monthly Notices Royal Astron. Soc.*, 446, 3820
- Goddard D., Thomas D., Maraston C., Westfall K., Etherington J., Riffel R., Mallmann N. D., Zheng Z., Argudo-Fernandez M., Bershady M. A., Bundy K., Drory N., Law D. R., Yan R., Wake D., Weijmans A.-M., Bizyaev D., Brownstein J. R., Lane R. R., Maiolino R., Masters K. L., Merrifield M. R., Nitschelm C., Pan K., Roman-Lopes A., Storchi-Bergmann T., 2016, ArXiv e-prints
- González J. J., 1993, PhD thesis, Thesis (PH.D.)—UNIVERSITY OF CALIFORNIA, SANTA CRUZ, 1993. Source: Dissertation Abstracts International, Volume: 54-05, Section: B, page: 2551.
- Greggio L., Renzini A., 2012, ArXiv:1205.1221
- Hopkins P. F., 2013, *Monthly Notices Royal Astron. Soc.*, 433, 170
- Horne K., 1986, *Pub. Astron. Soc. Pacific*, 98, 609
- Johansson J., Thomas D., Maraston C., 2012, *Monthly Notices Royal Astron. Soc.*, 421, 1908
- Kim D.-W., Fabbiano G., Brassington N. J., Fragos T., Kalogera V., Zezas A., Jordán A., Sivakoff G. R., Kundu A., Zepf S. E., Angelini L., Davies R. L., Gallagher J. S., Juett A. M., King A. R., Pellegrini S., Sarazin C. L., Trinchieri G., 2009, *Astrophys J.*, 703, 829
- Kinney A. L., Calzetti D., Bohlin R. C., McQuade K., Storchi-Bergmann T., Schmitt H. R., 1996, *Astrophys J.*, 467, 38
- Kroupa P., 2001, *Monthly Notices Royal Astron. Soc.*, 322, 231
- Krumholz M. R., 2014, *Physics Reports*, 539, 49
- La Barbera F., Ferreras I., Vazdekis A., de la Rosa I. G., de Carvalho R. R., Trevisan M., Falcón-Barroso J., Ricciardelli E., 2013, *Monthly Notices Royal Astron. Soc.*, 433, 3017
- Larson R. B., 1998, *Monthly Notices Royal Astron. Soc.*, 301, 569
- , 2005, *Monthly Notices Royal Astron. Soc.*, 359, 211
- Lee H.-c., Worthey G., Dotter A., Chaboyer B., Jevremović D., Baron E., Briley M. M., Ferguson J. W., Coelho P., Trager S. C., 2009, *Astrophys J.*, 694, 902
- Maraston C., 2005, *Monthly Notices Royal Astron. Soc.*, 362, 799
- Marigo P., Girardi L., Bressan A., Groenewegen M. A. T., Silva L., Granato G. L., 2008, *Astron. Astrophys.*, 482, 883
- Marks M., Kroupa P., Dabringhausen J., Pawlowski M. S., 2012, *Monthly Notices Royal Astron. Soc.*, 422, 2246
- Martín-Navarro I., Barbera F. L., Vazdekis A., Falcón-Barroso J., Ferreras I., 2015a, *Monthly Notices Royal Astron. Soc.*, 447, 1033
- Martín-Navarro I., Pérez-González P. G., Trujillo I., Esquej P., Vazdekis A., Domínguez Sánchez H., Barro G., Bruzual G., Charlot S., Cava A., Ferreras I., Espino N., La Barbera F., Koekemoer A. M., Cenarro A. J., 2015b, *Astrophys J. Letters*, 798, L4
- Miller G. E., Scalo J. M., 1979, *Astrophys J. Supplement Series*, 41, 513
- Neff S. G., Eilek J. A., Owen F. N., 2015, *Astrophys J.*, 802, 88
- Newman J. A., Cooper M. C., Davis M., Faber S. M., Coil A. L., Guhathakurta P., Koo D. C., Phillips A. C., Conroy C., Dutton A. A., Finkbeiner D. P., Gerke B. F., Rosario D. J., Weiner B. J., Willmer C. N. A., Yan R., Harker J. J., Kassin S. A., Konidaris N. P., Lai K., Madgwick D. S., Noeske K. G., Wirth G. D., Connolly A. J., Kaiser N., Kirby E. N., Lemaux B. C., Lin L., Lotz J. M., Luppino G. A., Marinoni C., Matthews D. J., Metevier A., Schiavon R. P., 2013, *Astrophys J. Supplement Series*, 208, 5
- Offner S. S. R., Clark P. C., Hennebelle P., Bastian N., Bate M. R., Hopkins P. F., Moraux E., Whitworth A. P., 2014, *Protostars and Planets VI*, 53
- Peacock M. B., Zepf S. E., Maccarone T. J., Kundu A., Gonzalez A. H., Lehmer B. D., Maraston C., 2014, *Astrophys J.*, 784, 162
- Peek J. E. G., Graves G. J., 2010, *Astrophys J.*, 719, 415
- Poole V., Worthey G., Lee H.-c., Serven J., 2010, *Astron. J.*, 139, 809
- Posacki S., Cappellari M., Treu T., Pellegrini S., Ciotti L., 2015, *Monthly Notices Royal Astron. Soc.*, 446, 493
- Rayner J. T., Cushing M. C., Vacca W. D., 2009, *Astrophys J. Supplement Series*, 185, 289
- Ross A. J., Beutler F., Chuang C.-H., Pellejero-Ibanez M., Seo H.-J., Vargas-Magaña M., Cuesta A. J., Percival W. J., Burden A., Sánchez A. G., Grieb J. N., Reid B., Brownstein J. R., Dawson K. S., Eisenstein D. J., Ho S., Kitaura F.-S., Nichol R. C., Olmstead M. D., Prada F., Rodríguez-Torres S. A., Saito S., Salazar-Albornoz S., Schneider D. P., Thomas D., Tinker J., Tojeiro R., Wang Y., White M., Zhao G.-b., 2016, *Monthly Notices Royal Astron. Soc.*
- Salpeter E. E., 1955, *Astrophys J.*, 121, 161
- Sánchez-Blázquez P., Peletier R. F., Jiménez-Vicente J., Cardiel N., Cenarro A. J., Falcón-Barroso J., Gorgas J., Selam S., Vazdekis A., 2006, *Monthly Notices Royal Astron. Soc.*, 371, 703
- Scalo J. M., 1986, *Fundam. Cosmic Phys.*, 11, 1
- Schiavon R. P., Faber S. M., Konidaris N., Graves G., Willmer C. N. A., Weiner B. J., Coil A. L., Cooper M. C., Davis M., Harker J., Koo D. C., Newman J. A., Yan R., 2006, *Astrophys J. Letters*, 651, L93
- Serven J., Worthey G., 2010, *Astron. J.*, 140, 152
- Serven J., Worthey G., Briley M. M., 2005, *Astrophys J.*, 627, 754
- Shetty S., Cappellari M., 2014, *Astrophys J. Letters*, 786, L10
- Smith R. J., Alton P., Lucey J. R., Conroy C., Carter D., 2015, *Monthly Notices Royal Astron. Soc.*, 454, L71
- Smith R. J., Lucey J. R., Carter D., 2012, *Monthly Notices Royal Astron. Soc.*, 426, 2994
- Spiniello C., Trager S., Koopmans L. V. E., Conroy C., 2014, *Monthly Notices Royal Astron. Soc.*, 438, 1483
- Spiniello C., Trager S. C., Koopmans L. V. E., 2015, *Astrophys J.*, 803, 87
- Tang B., Worthey G., 2015, *Monthly Notices Royal Astron. Soc.*, 453, 4431
- Tang B., Worthey G., Davis A. B., 2014, *Monthly Notices Royal Astron. Soc.*, 445, 1538
- Tang B.-T., Gu Q.-S., Huang S., 2009, *Research in Astronomy and Astrophysics*, 9, 1215
- Tinsley B. M., Gunn J. E., 1976, *Astrophys J.*, 203, 52

- Tonry J., Davis M., 1979, *Astron. J.*, 84, 1511
- Trager S. C., Faber S. M., Worthey G., González J. J., 2000a, *Astron. J.*, 120, 165
- , 2000b, *Astron. J.*, 119, 1645
- Trager S. C., Worthey G., Faber S. M., Burstein D., González J. J., 1998, *Astrophys J. Supplement Series*, 116, 1
- Valdes F., Gupta R., Rose J. A., Singh H. P., Bell D. J., 2004, *Astrophys J. Supplement Series*, 152, 251
- van Dokkum P., Conroy C., Villaume A., Brodie J., Romanowsky A., 2016, ArXiv e-prints
- van Dokkum P. G., 2008, *Astrophys J.*, 674, 29
- van Dokkum P. G., Conroy C., 2010, *Nature*, 468, 940
- Weidner C., Ferreras I., Vazdekis A., La Barbera F., 2013a, *Monthly Notices Royal Astron. Soc.*, 435, 2274
- Weidner C., Kroupa P., Pflamm-Altenburg J., Vazdekis A., 2013b, *Monthly Notices Royal Astron. Soc.*, 436, 3309
- Weiner B. J., Phillips A. C., Faber S. M., Willmer C. N. A., Vogt N. P., Simard L., Gebhardt K., Im M., Koo D. C., Sarajedini V. L., Wu K. L., Forbes D. A., Gronwall C., Groth E. J., Illingworth G. D., Kron R. G., Rhodes J., Szalay A. S., Takamiya M., 2005, *Astrophys J.*, 620, 595
- Whitmore B. C., Kirshner R. P., 1981, *Astrophys J.*, 250, 43
- Worthey G., 1994, *Astrophys J. Supplement Series*, 95, 107
- , 1998, *Pub. Astron. Soc. Pacific*, 110, 888
- Worthey G., Danilet A. B., Faber S. M., 2014a, *Astron. Astrophys.*, 561, A36
- Worthey G., Faber S. M., Gonzalez J. J., Burstein D., 1994, *Astrophys J. Supplement Series*, 94, 687
- Worthey G., Tang B., Serven J., 2014b, *Astrophys J.*, 783, 20
- Zheng Z., Wang H., Ge J., Mao S., Li C., Li R., Mo H., Goddard D., Bundy K., Li H., Nair P., Lin L., Long R. J., Riffel R., Thomas D., Masters K., Bizyaev D., Brownstein J. R., Zhang K., Law D. R., Drory N., Lopes A. R., Malanushenko O., 2016, ArXiv e-prints